Energy-Efficient Capacitive Deionization through Electrode Modification and Process Development

Lauren Valentino[a]*, *Lily Callen*[a#], *Samantha Kelly*[a$], *Sungjoon Kim*[a]

[a]Applied Materials Division, Argonne National Laboratory, Lemont, IL, 60439, USA

*Corresponding author [phone: +1 630 252 5029; e-mail: lvalentino@anl.gov]

ABSTRACT

Electrochemical separation technologies, such as capacitive deionization (CDI), are promising for addressing global energy and water challenges. However, there is a need to improve the performance, better understand property-performance relationships, and evaluate the longevity of CDI electrodes. This study explores the chemical modification of electrodes and the adjustment of CDI operating parameters. Results indicate that nitric acid (HNO_3) conditioning of activated carbon cloth (ACC) electrodes removes metal oxides, introduces oxygen and nitrogen functionalities, and increases the specific capacitance (16% at 1 mV/s). Moreover, these changes in electrode properties positively impact device-level CDI performance. Through HNO_3-conditioning of the ACC and tuning of the operational parameters, this work demonstrates higher electrosorption capacity (4.0×), greater charge efficiency (90% vs. 24%), and lower energy consumption (3.8×). Despite these enhancements, limitations of the HNO_3-conditioned ACC include decreased desorption kinetics and a 32% loss in electrosorption capacity after 200 cycles. Overall, this work provides guidance on using oxidative pretreatment via HNO_3 to modify ACC electrodes for CDI and evaluates the tradeoffs associated with varying operational parameters.

KEYWORDS

Separation, Electrosorption, Activated carbon, Pretreatment, Flow rate, Half-cycle time

INTRODUCTION

Electrification has been recognized as a key strategy for mitigating greenhouse gas emissions and decarbonizing energy supply chains.[1,2] In line with this paradigm shift, electrochemical separation technologies, including capacitive deionization (CDI), that eliminate the need for high pressures or temperatures are gaining attention for low salinity deionization and resource recovery applications. CDI involves the application of an electric potential across a pair of porous electrodes, creating an electric field that drives ion transport towards oppositely charged electrodes as shown in Figure S1. Ions are electrostatically immobilized and stored capacitively in the electrical double layers (EDLs) within the electrode micropores, resulting in salt extraction from solution. The electrodes are then regenerated by removing or reversing the potential. CDI usually operates through a cyclic process to extract and recover ions. A typical CDI cell is comprised of porous carbon-based electrodes that are separated by a spacer, allowing feed solution to flow along the surface of the electrodes.[3-5] Activated carbon is particularly attractive for CDI because of its high specific surface area (S_{BET}), porosity, commercial availability,[6,7] and low cost relative to other carbon materials.

Several strategies have been employed to further enhance the properties of activated carbon for CDI.[8,9] In particular, nitric acid (HNO_3) has been used to modify the surface chemistry by introducing Oxygen (O)-containing functional groups,[10-14] which are known to increase the specific capacitance (C_s).[15-18] Previous studies have employed HNO_3-conditioned electrodes in CDI and demonstrated enhanced ion extraction and kinetics; however, these studies lack

comprehensive evaluation of other performance metrics, *e.g.*, charge efficiency (Λ) and specific energy consumption (E).[19,20] Only two studies have reported data for adsorption capacity (Γ_A) and Λ, but they are limited to a single HNO_3 exposure.[21,22] While other studies have reported HNO_3 pretreatment of CDI electrodes,[23-26] they do not specifically evaluate the impacts of pretreatment.

CDI performance is also largely dependent on the operating parameters. Using a constant voltage of 1.2 V provides a high driving force while minimizing undesirable side reactions.[7,27] In general, Γ_A increases as charging time increases, but the average salt adsorption rate ($\bar{r}_A$) decreases.[27,28] Previous work has shown that increasing the flow rate can enhance Γ_A, but beyond a certain threshold, increases in flow rate reduce Γ_A due to insufficient contact time.[29,30] Since there is not a singular indicator of performance in CDI, assessing the optimal operating conditions is complex, and unoptimized operation can lead to inefficiencies that are detrimental to process feasibility. In addition, among the studies that implemented HNO_3-conditioned activated carbon for CDI, none have examined the impact of varying the flow rate or half-cycle time (HCT).

This study assesses the effects of HNO_3 modification on the performance of activated carbon cloth (ACC) electrodes in CDI and further explores the synergy between these modifications and key operating parameters, specifically flow rate and HCT. Changes to the surface morphology and topology, chemical composition, electrochemical and porous properties, and CDI performance were assessed. Aside from the introduction of O- and Nitrogen (N)-containing groups, this study uniquely demonstrates the benefit of using HNO_3 to remove residual metal oxides from the ACC along with a limitation regarding decreased desorption kinetics. After establishing the optimal pretreatment solution, CDI operating parameters were varied to further enhance separation performance. This is the first study to examine the combined effects of electrode modification and varying operating conditions on the performance of CDI. In addition,

the longevity of the electrodes was assessed by monitoring a range of CDI performance metrics over 200 continuous cycles. Through this investigation, this work advances both foundational and applied principles related to CDI for deionization applications and is essential for scaling up and transitioning CDI from bench-scale to larger-scale applications.

METHODS

Materials and Reagents

Commercially available ACC (Flexzorb FM10, Chemviron Carbon, Houghton le Spring, UK) was modified by immersing in one of 6 solutions: Milli-Q water (18.2 MΩ-cm resistivity), 1-4 M HNO_3, or 3 M sodium nitrate ($NaNO_3$) for 24 h. After thorough rinsing, ACC was cut to size, dried for 24 h at 100 °C, and weighed immediately after removal from the oven. The manufacturer specifications for FM10 and pretreatment conditions are provided in Tables S1 and S2. ACS reagent grade HNO_3 (70%) and sodium chloride (NaCl; ≥99.0%) were obtained from Sigma Aldrich (St. Louis, MO) and Fisher Scientific (Waltham, MA), respectively, and diluted or dissolved using Milli-Q water.

Analytical Characterization Techniques

X-ray photoelectron spectroscopy (XPS) was performed using a K-Alpha+ spectrometer (Thermo Fisher Scientific, Waltham, MA) with a monochromatic Al Kα X-ray source (1487 eV) and a 400 μm spot size. ACC was adhered to conductive Copper tape to minimize sample charging, survey spectra were collected using a pass energy of 200 eV and a step size of 1 eV, and high-resolution scans were collected with a pass energy of 50 eV and a step size of 0.1 eV. Data interpretation was performed by Thermo Fisher Avantage software with each measurement representing an average of 5 scans. All spectra were calibrated with the C1s peak at 284.8 eV.

Nitrogen (N_2) gas sorption isotherms were measured at -196 °C using a surface area and porosity analyzer (3Flex, Micromeritics Instrument Corporation, Norcross, GA) after degassing at 100 °C for 24 h. S_{BET} and the pore size distribution were determined using Brunauer–Emmett–Teller (BET) theory and the Non-Local Density Functional Theory (NLDFT) model, respectively. S_{BET} was calculated using the adsorption data with Rouquerol criteria.[31] The total pore volume (V_{tot}) was calculated using the adsorption data and the carbon slit-pore model for N_2 at 77 K.

Cyclic voltammetry (CV) was performed by scanning from -0.5 to 0.5 V using a range of scan rates (k; 1-5 mV/s). The working electrode, a 3 cm^2 swatch of ACC, was mounted on a Platinum sheet, installed in a custom-made holder, and immersed in 0.5 M NaCl for 24 h prior to measurements. A graphite rod and Ag/AgCl electrode were used as the counter and reference electrode, respectively. The electrolyte was sparged with N_2 gas before testing, and a low flow of gas was continually flushed into the headspace during measurements. C_s was calculated using Equation S1.

CDI Performance Evaluation

CDI experiments were conducted using a custom-built electrochemical cell (14 cm^2 active area), consisting of a pair of electrodes separated by 1.4 mm. Solution flowed between the electrodes (Figure S2) at a rate of 4-16 mL/min. A LabVIEW (National Instruments, Austin, TX) program was used for control and data acquisition along with a DC power supply and flow-through conductivity probe (ET908, eDAQ, Colorado Springs, CO). CDI performance is described by several performance metrics (Equations S2-S8), which were calculated for each cycle.

RESULTS AND DISCUSSION

Elemental and Functional Group Analysis

XPS of the 6 ACC materials reveals key components: Carbon, N, and O, for which elemental analysis is presented in Table 1. The full compositional analysis, provided in Table S3, includes Aluminum and Zinc. These metals, likely a residual from the commercial manufacturing process, are leached from the ACC during HNO_3 conditioning. This is confirmed by scanning electron microscopy (SEM), energy dispersive X-ray spectroscopy (EDS), and inductively coupled plasma optical emission spectroscopy (ICP-OES), as described in detail in the Supplementary Information (SI; Table S3 and Figures S3-S6).

Table 1. Elemental analysis in atomic (at.) % characterized by XPS, curve fitting of the O1s and N1s regions from XPS, and S_{BET} and V_{tot} for ACC conditioned in 3 M $NaNO_3$ (control, C), Milli-Q water (0), or 1-4 M HNO_3. XPS was performed using a 400 μm spot size and by averaging 5 individual scans to account for spatial variability. The values for S_{BET} and V_{tot} represent 2 measurements and are presented as the average ± standard deviation.

			[HNO_3] (M)					
			C	0	1	2	3	4
Elemental composition by XPS (at. %)	C		82.7	79.9	87.0	82.0	84.0	81.0
	N		1.6	1.5	2.0	2.1	2.4	2.1
	O		13.6	14.8	9.8	13.2	11.9	14.2
	O/C		0.16	0.19	0.11	0.16	0.14	0.18
Functional groups (at. %)	O1s	O-C=O	5.4	4.6	5.7	8.7	7.2	8.4
		C=O	7.5	9.6	3.6	3.9	4.1	4.9
		C-O	0.6	0.7	0.4	0.7	0.7	0.9
	N1s	N-6	0.1	0.3	0.2	0.1	0.1	0.1
		N-Q	1.5	1.2	1.5	1.6	1.7	1.3
		-NO2	-	-	0.3	0.4	0.7	0.8
Textural properties	S_{BET} (m^2/g)		1235 ± 29	1198 ± 0	1217 ± 4	1255 ± 45	1153 ± 1	1172 ± 13
	V_{tot} (cm^3/g)		0.53 ± 0.01	0.53 ± 0.03	0.54 ± 0.03	0.57 ± 0.04	0.50 ± 0.01	0.52 ± 0.01

125 The data in Table 1 show that as [HNO_3] increases from 1 to 4 M, there is an increase in
126 surface O concentration. Further, the O/C ratio, which can be used as an indicator of surface
127 oxidation, increases by 64%. Previous work has shown that the aliphatic chains are particularly
128 susceptible to oxidation, producing carboxylic and ketone groups.[10] After curve fitting of the high-
129 resolution O1s spectra (Figures 1 and S7), there are increases in carboxylic (O-C=O), carbonyl
130 (C=O), and alcohol/ether (C-O) groups as [HNO_3] increases from 1 M to 4 M. It is well established
131 that the presence of these functional groups contributes to surface acidity.[17,32] These groups also
132 increase the surface charge density and hydrophilicity, which can enhance Γ_A.[8,14,33] This is because
133 EDLs, the primary mechanism through which ions are removed in CDI, can only be formed at
134 solution-electrode interfaces,[34] so higher wettability facilitates greater infiltration of the electrolyte
135 into the porous ACC.[7,9]

136 Table 1 also reveals a slight increase in N, which is consistent with literature,[12,35-38]
137 although most studies focus on the incorporation of O-containing groups. After curve fitting, all
138 high-resolution N1s spectra include a peak at ~401 eV that is attributed to aromatic amines (N-
139 Q)[39] and a peak at ~398 eV that is associated with more reduced, pyridinic nitrogen (N-6).[37,39-41]
140 In comparison to the ACC conditioned in water and $NaNO_3$, the spectra for the ACC conditioned
141 in 1-4 M HNO_3 exhibit a unique peak at ~406 eV, associated with nitro groups (-NO_2).[37,39-41] The
142 emergence of this peak is further illustrated in Figure S8a. The residuals from the spectral fitting
143 are plotted in Figure S8b to demonstrate that the spectra for ACC conditioned with Milli-Q water
144 and 3 M $NaNO_3$ are adequately represented without the nitro group peak at 406 eV. Both -NO_2
145 and N-6 functional groups can enhance the wettability and C_s of electrodes,[42,43] including activated
146 carbon.[40,44] Overall, these results directly link HNO_3 conditioning to ACC oxidation, marking the
147 first report connecting -NO_2 functionalization of ACC to enhanced CDI performance. Finally,

148 although Fourier transform infrared (FTIR) spectroscopy was performed, the analysis reveals no
149 obvious differences. Additional detail about the FTIR methodology and results are presented in
150 the SI (Figure S9).

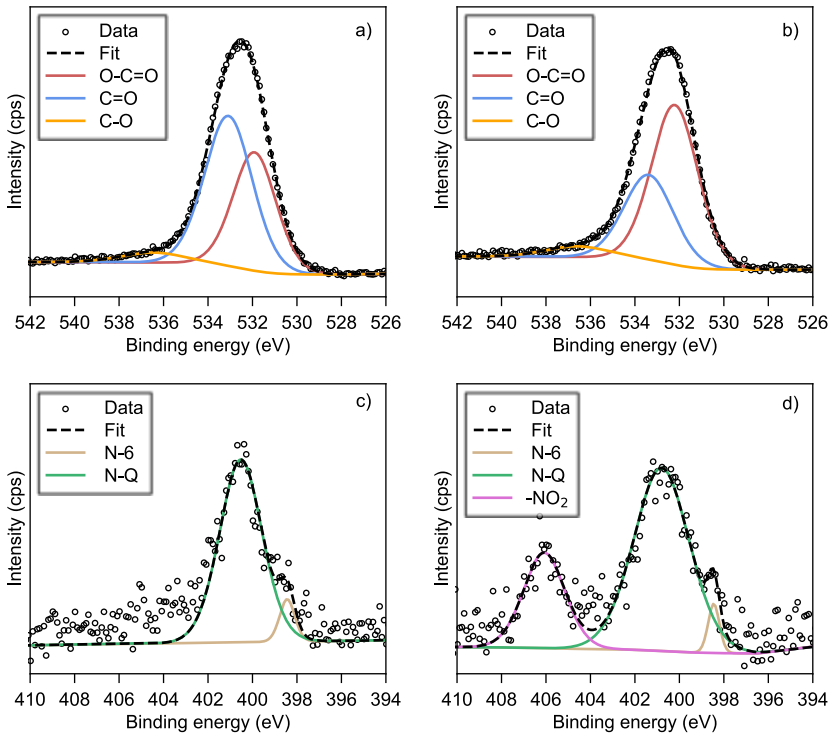

151

152 Figure 1. Representative O1s and N1s spectra for ACC conditioned with a and c) 3 M $NaNO_3$ and
153 b and d) 3 M HNO_3. Three components (O1s: O-C=O, C=O, and C-O and N1s: N-6, N-Q, and -
154 NO_2) were applied for O1s and N1s spectral fitting.

155

156 Electrochemical Characterization

157 Figure 2 shows the CV characterization results at various *k* (1-5 mV/s). The
158 voltammograms collected using lower *k* have semi-rectangular shapes that are typically associated
159 with EDL capacitors. In addition to EDL capacitance, small pseudocapacitive contributions are
160 observed for all ACCs. These are more pronounced for ACC conditioned with 2-4 M HNO_3

(Figures 2a and 2b), and the slight shift in the pseudocapacitive peak position is consistent with changes to the electrode surface observed by XPS. Similar pseudocapacitive peaks have been reported in literature for HNO_3-treated activated carbon.[20,40] Specifically, the presence of N and O functional groups on the surface of carbon materials has been reported to induce pseudocapacitance or redox activity.[40,42-44] Additionally, as *k* increases, the current response, *i.e.*, current density (*J*), increases. The CVs for ACCs conditioned with $NaNO_3$ and water maintain the same general shape. However, consistent with published literature,[8,19,25] the ACCs conditioned with 2-4 M HNO_3 appear more lens-shaped at 5 mV/s, suggesting greater deviation from ideal capacitive behavior.

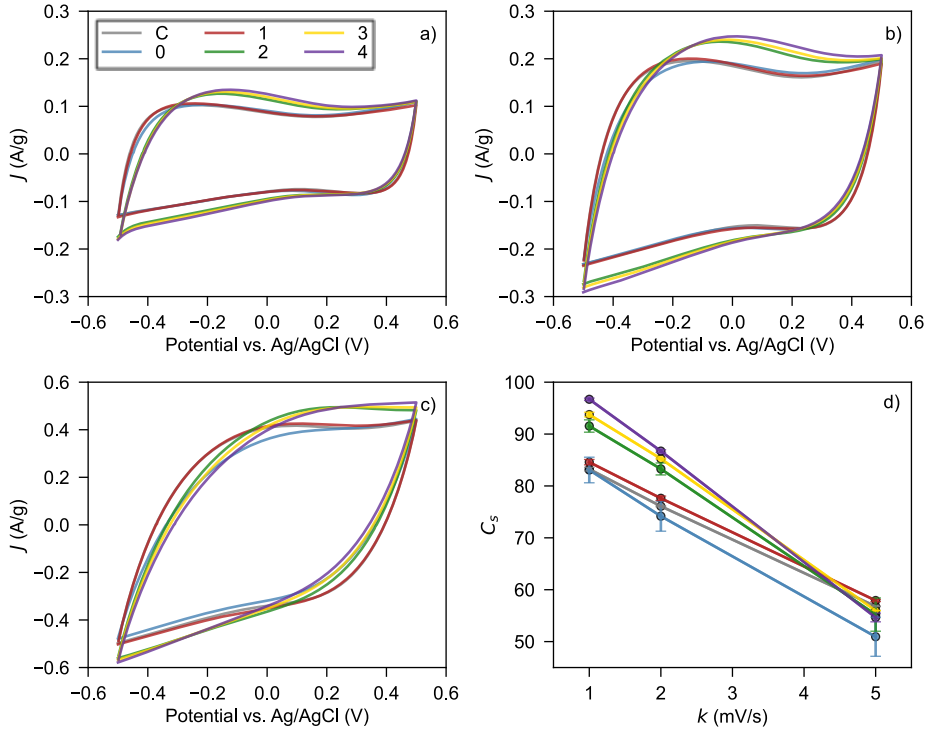

Figure 2. Representative voltammagrams collected at a) k = 1 mV/s, b) k = 2 mV/s, and c) k = 5 mV/s in addition to d) C_s vs. k for ACC conditioned in 3 M $NaNO_3$ (C), Milli-Q water (0), or 1-4

M HNO_3 (1-4). The error bars in panel (d) represent the standard deviation of 2-6 measurements for each condition.

The underlying motivation for electrode modification is increasing C_s, which is directly related to Γ_A,[45] and Figure 2d shows an inverse relationship between C_s and k. Scanning slowly provides more time for diffusion, allowing enhanced contact between electrolyte ions and the internal surface of the electrode. As a result, greater charge storage leads to higher C_s. Conversely, when k increases, the time scale limits mass transfer into the smallest pores resulting in less charge storage and low C_s.[25,46] In other words, the microporosity limits the accessibility of electrolyte ions at high k. As shown in Figure 2d, at the highest k, the ACC conditioned in 1 M HNO_3 and Milli-Q water show the highest and lowest C_s, respectively. However, at the lowest k of 1 mV/s, C_s increases with [HNO_3], with an overall 16% increase in the 0-4 M range. These measurements at different k provide insight into the contributions of pores of different sizes and suggest that micropore accessibility plays a key role in charge storage for these ACC materials. The change in slope for C_s vs. k when [HNO_3] > 1 M also suggests a change in the charging mechanism, which is further supported by the introduction of N and O functionalities and the more pronounced pseudocapacitive peaks following ACC conditioning with 2-4 M HNO_3.

Finally, although it is often assumed that the key to achieving high C_s through EDL charging is high S_{BET}, there is no clear relationship between these two properties for the ACC investigated in this study. A lack of correlation has also been observed by others.[47,48] While high S_{BET} generally indicates more surface area available for charge storage, the surface chemistry also plays a role in determining C_s. Table 1 shows a systematic increase in S_{BET} from 0 to 2 M HNO_3, followed by a decrease after exposure to higher concentrations, reflecting the competing effects of surface functionalization and porous characteristics. After lower exposures, HNO_3 enhances S_{BET}

196 by introducing functional groups and potentially etching micropores. At higher concentrations,
197 excessive oxidation may cause structural damage, leading to a reduction in S_{BET}. Overall, for the
198 ACC in this study, C_s is more sensitive to variations in surface chemistry than S_{BET}. In other words,
199 the enhanced Faradaic activity and/or wettability provided by oxygenated and nitro functional
200 groups outweigh the effects of reduced S_{BET}. In addition to S_{BET}, the results for V_{tot} are presented
201 in Table 1; additional discussion and the isotherms are provided in the SI (Figure S10).

202 CDI Performance

203 With increased surface functionality and C_s, this study incorporated the HNO_3-conditioned
204 ACC in an electrochemical cell to evaluate E and Λ, along with other performance metrics. All
205 CDI experiments were performed using NaCl solution because it is highly relevant for water
206 treatment and energy production applications. Aside from being a major contributor to salinity in
207 various aqueous environments, inorganic salts can have a detrimental effect on product recovery
208 and catalytic upgrading in bioenergy conversion,[49] so techniques for extraction/recovery are key.

209 *Effects of HNO_3 Conditioning*

210 To investigate the effects of HNO_3 pretreatment on electrochemical separation
211 performance, CDI experiments were carried out using a symmetric electrode configuration. Fifteen
212 cycles were conducted to ensure dynamic equilibrium, and all experiments were conducted in
213 duplicate using separate sets of electrodes. Figure S11a shows a representative effluent
214 concentration ($[Cl^-]_e$) profile for a single CDI cycle from each experiment. Each $[Cl^-]_e$ data set was
215 normalized by subtracting the influent concentration ($[Cl^-]_0$) to obtain the net reduction or increase
216 in ion concentration during adsorption and regeneration, respectively. Comparing the $[Cl^-]_e - [Cl^-]_0$
217 profiles reveals notable differences in the change in concentration over the cycle. To further
218 investigate this, concentration data were extracted for discrete time intervals, illustrated by the

dashed lines in Figure S11a. For each time interval, the slope of the $[Cl^-]_e - [Cl^-]_0$ vs. time curve was calculated, providing a quantitative measure of the instantaneous adsorption or desorption rate (r_A or r_D) within a given time interval. The results are presented in Figures S11b and S11c. At the beginning of the cycle, r_A is 10-24× greater for the 2, 3 and 4 M HNO_3-pretreated electrodes in comparison to the electrodes conditioned in water, 3 M $NaNO_3$, and 1 M HNO_3. Looking at the concentration profiles in Figure S11a and r_D in Figure S11c, all data sets show a rapid concentration increase at the beginning of the discharging step, aligning with expectations for a purely electrostatic process. However, at ~730 s, the rates for the 2 M, 3 M, and 4 M-conditioned electrodes slow. Overall, the differences in r_D suggest that other factors may be influencing the ion release dynamics. While other studies have reported enhanced adsorption kinetics using HNO_3-conditioned ACC,[19,20] this is the first report of slower discharge kinetics.

Equations S2-S8 were used to further evaluate the CDI performance. As shown in Figure 3, Γ_A, $\bar{r}_A$, and Λ increase while E decreases when electrodes are pretreated with HNO_3. In contrast, the control experiments, performed with $NaNO_3$-conditioned electrodes, show marginal improvements to the performance metrics. Initially, as $[HNO_3]$ increases, the performance improves but then plateaus at 2 M. In other words, conditioning with 3 or 4 M HNO_3 does not lead to further performance enhancements. This behavior indicates that there is an optimal exposure for HNO_3 pretreatment beyond which higher concentrations do not provide additional improvements. Since 2 M HNO_3 is equally as effective as 4 M HNO_3, there are several reasons why a lower acid concentration pretreatment is desirable. For example, using a lower acid concentration simplifies the conditioning and rinsing procedure, poses fewer safety risks, incurs less cost, minimizes waste generation, and facilitates scale up since handling and processing large volumes of lower concentration acids are more manageable. Overall, Figure 3 shows that Γ_A and $\bar{r}_A$ increase by up

to 3.5× following HNO_3 pretreatment. Similarly, E decreases by 3.5×, and Λ increases from as low as 24% to 82%. Notably, these performance enhancements were achieved through electrode pretreatment alone, effectively scaling the technology without increasing the physical footprint of the CDI cell.

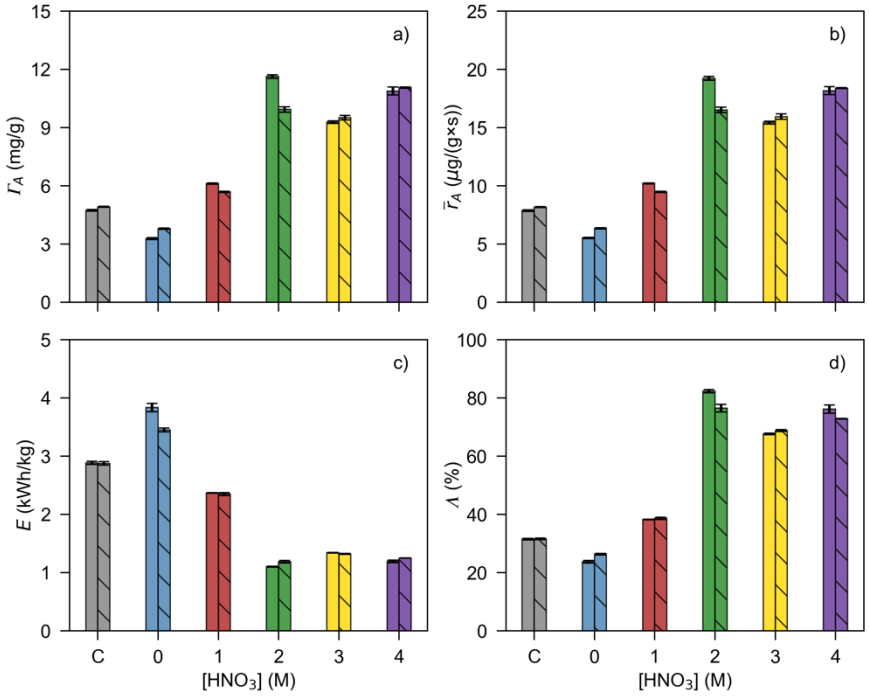

Figure 3. a) Γ_A, b) $\bar{r}_A$, c) E, and d) Λ for each CDI experiment conducted using electrodes conditioned in 3 M $NaNO_3$ (C), water (0), or 1-4 M HNO_3. Each bar represents one of two duplicate experiments (solid and hatched), and the error bars represent the standard deviation of each metric over the last 5 cycles of operation.

Effects of Operating Parameters

Aside from electrode material, CDI performance is sensitive to operating variables, *e.g.*, voltage, flow rate, and time. Previous studies have well-established that 1.2 V is optimal for effective ion removal while minimizing side reactions.[7,27] As such, this study does not investigate

multiple voltage conditions. Rather, this work evaluates the effects of flow rate and HCT. Focusing on HCT (the duration of either the charging or discharging phase) rather than total cycle time (the sum of both the charging and discharging steps) emphasizes the charging phase, which is the key period for monitoring adsorption/extraction in CDI.

Having established 2 M HNO_3 as the optimal conditioning solution, experiments were conducted with a range of flow rates (4, 8, and 16 mL/min) and HCTs (5, 10, and 15 min). Note that in this study, the charging and discharging steps are of the same duration, so HCT is half of the total cycle time. The results are provided in Figure 4 and Table S4. For a given flow rate, increasing the HCT leads to greater Γ_A until the maximum capacity is reached (*i.e.*, 12.5-13 mg/g) and lower $\bar{r}_A$ as shown in Figure 4a. Alternatively, for a fixed HCT, increasing the flow rate enables the system to reach equilibrium more quickly. With a short HCT of 5 min, increasing the flow rate from 4 to 16 mL/min increases Γ_A by 26%, but coupling longer HCT with higher flow rates does not provide additional gains because the electrodes saturate. As shown in Figure 4b, the combination of 16 mL/min and 5 min HCT provides the lowest E (1.0 kWh/kg) and highest Λ (90%), but Γ_A is <70% of the maximum value. Doubling HCT increases Γ_A to 97% of the maximum value, but E increases by 10-15%. In general, longer HCT results in higher E because the electrodes are charged for a longer period of time. As the electrodes approach equilibrium, extended charging becomes increasingly inefficient. The ion adsorption kinetics slow until no additional ions can be extracted. Balancing this tradeoff is critical; shorter cycles can save energy but may leave Γ_A underutilized, while longer cycles maximize Γ_A but risk inefficient energy use. Overall, understanding these tradeoffs is key to the scale up and implementation of CDI systems because E is directly related to the operational cost and environmental impacts.

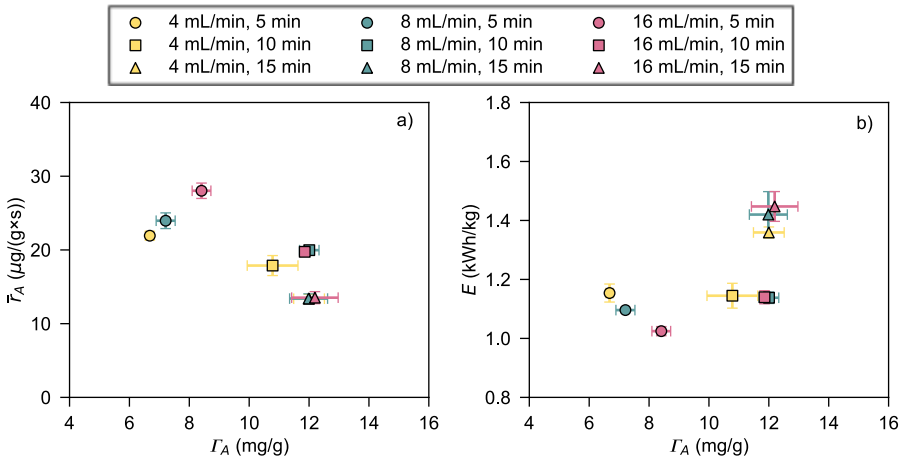

278

279 Figure 4. Effects of flow rate and HCT on CDI performance showing the tradeoff between a) Γ_A
280 and $\bar{r}_A$ and b) Γ_A and E. Each experiment was replicated, and the symbols and error bars represent
281 the average and standard deviation, respectively, of duplicates.

282

283 To tailor CDI systems for specific applications beyond NaCl extraction, experimental
284 designs should account for whether maximizing Γ_A or minimizing E is the primary objective. For
285 applications prioritizing Γ_A, longer HCT can be combined with moderate to high flow rate. For
286 applications focused on minimizing E, shorter cycles with a higher flow rate will utilize the most
287 efficient phase of adsorption. In many cases, the goal is to simultaneously maximize Γ_A while
288 minimizing E, making the energy-capacity tradeoff plot (Figure 4b) an especially useful and
289 practical tool for optimizing CDI systems. Finally, in this study, the highest flow rate (16 mL/min)
290 yielded favorable results, but it is important to note that excessively high flow rates may reduce
291 contact time and limit ion removal efficiency.

292 *Electrode longevity*

293 Despite beneficial short-term improvements in this work and a previous study concluding
294 that CDI with HNO_3-conditioned ACC electrodes shows better cyclability than with untreated

ACC,[21] others have shown that oxygenated functional groups are detrimental to the cyclability of carbon-based supercapacitors.[50] To investigate the impacts on the long-term stability in CDI, electrosorption was tracked over 200 cycles using 2 M HNO_3-conditioned ACC, a flow rate of 4 mL/min, and HCT of 10 min. The results are presented in Figure 5. The overlay of effluent concentration profiles shown in Figure 5a illustrates the time evolution of ion removal and recovery. Figures 5b and S12 show that Γ_A and desorption decrease as the number of cycles increases despite maintaining ~100% recovery. Note that data from the initial cycles are not representative because the system has not yet reached dynamic equilibrium. Over the 200 cycles, Γ_A decreases by 32% from 10.4 mg/g to 7.1 mg/g. This is comparable to previous work that observed a 25% decrease in Γ_A after 200 CDI cycles using water-washed ACC.[51] However, it is important to note that the ACC used in that study was different, the cycles were shorter (4 vs. 20 min), and the flow rate was slightly higher (7 vs 4 mL/min).

Lower Γ_A results in higher E and lower Λ, as shown in Figures 5c and 5d. Essentially, more energy is consumed for less effective ion capture, leading to lower process efficiency. These observations suggest that the findings from supercapacitor research can be extended to CDI. This study highlights the need for further optimization to balance the initial performance with the longevity required for practical deionization applications. Finally, although the primary focus of this study is to investigate the effects of electrode conditioning on performance, including the potential for sustaining the improvement observed in the short-term over hundreds of cycles, future research should focus on further characterizing the degradation mechanisms associated with cycling.

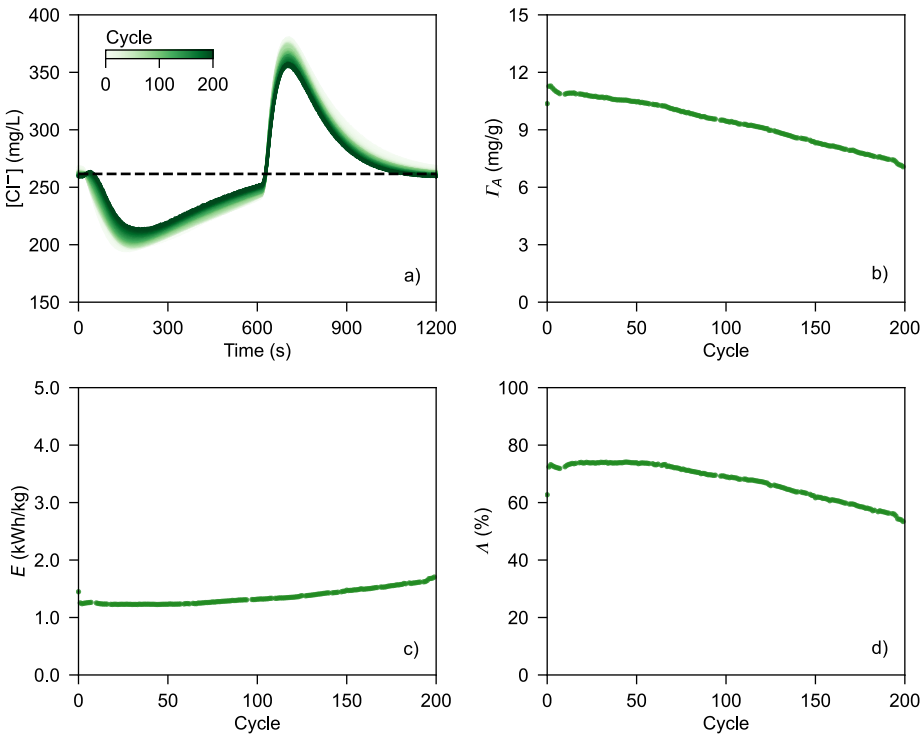

316

317 Figure 5. a) Overlay of effluent concentration profiles from a continuous CDI run of 200 cycles
318 using 2 M HNO_3-pretreated electrodes. The dashed line shows the influent concentration, and the
319 color gradient represents cycle progression. Performance metrics b) Γ_A, c) E, and d) Λ for each of
320 the 200 cycles.

CONCLUSIONS

This study presents a comprehensive analysis that simultaneously evaluates the effects of HNO_3 conditioning and varying operating conditions on the performance of ACC in CDI systems. After relatively low HNO_3 exposure (2 M for 24 h), charge-discharge cycling experiments demonstrate significant improvements in Γ_A, Λ, and E, attributed to the introduction of O and N-containing functional groups and increased C_s. With the exception of the desorption rate, the changes in surface chemistry and C_S from HNO_3 conditioning are linked to positive improvements in CDI performance, including higher Γ_A, greater Λ, and reduced E. This approach highlights the potential for optimizing existing CDI systems for better performance while maintaining original device size and design, thus facilitating integration into current applications. In addition, this study fine-tuned the operating conditions to further improve E and Λ, surpassing those reported in previous studies. Finally, this work investigated a critical aspect that has been largely overlooked in CDI literature: the long-term performance of HNO_3-conditioned ACC electrodes. Initially appearing to stabilize after ~10 cycles, monitoring of the effluent over 200 continuous CDI cycles reveals a gradual decline of all performance metrics, *e.g.*, decreasing Γ_A and Λ and increasing E. Future research should focus on understanding the mechanisms of degradation during cycling and developing strategies to mitigate these effects. In summary, by investigating the effects of HNO_3 pretreatment and operational variables, this study provides valuable insights that can facilitate the scale up and transition of CDI technology into commercial settings. The findings offer guidance for design decisions and operational strategies, ultimately leading to enhanced efficiency and effectiveness in chemical separation processes.

SUPPORTING INFORMATION

Electrode charging and discharging; Manufacturer specifications for the ACC; Pretreatment, rinsing, and drying conditions; Calculation of C_s; Electrochemical cell configuration; Calculation of CDI performance metrics; Elemental concentrations for ACC; SEM and EDS methods and results; ICP-OES method and results; XPS curve fitting and stacked N1s spectra; FTIR method and results; Adsorption/desorption isotherms; Normalized CDI effluent concentrations; CDI performance at different flow rates and HCTs; Long-term CDI performance

ACKNOWLEDGEMENTS

This work was sponsored by the U.S. Department of Energy (DOE) Energy Efficiency and Renewable Energy (EERE) Bioenergy Technologies Office (BETO) through the Bioprocessing Separations Consortium under Contract DE-AC02-06CH11357. SEM and EDS were performed at the Center for Nanoscale Materials, a U.S. Department of Energy Office of Science User Facility, supported by the U.S. DOE, Office of Basic Energy Sciences under Contract No. DE-AC02-06CH11357.

PRESENT ADDRESSES

[#]L.C.: Department of Chemical and Biological Engineering, University of Wisconsin-Madison, Madison, WI, 53706, USA

[$]S.K.: Wisconsin Energy Institute, University of Wisconsin-Madison, Madison, WI, 53706, USA

REFERENCES

(1) International Energy Agency. *Net Zero by 2050*; OECD Publishing, 2021. DOI: 10.1787/c8328405-en.

(2) Kerry, J.; McKarthy, G. *The Long-Term Strategy of the United States: Pathways to Net-Zero Greenhouse Gas Emissions by 2050*; United States Department of State and the United States Executive Office of the President, 2021.

(3) Blair, J. W.; Murphy, G. W. Electrochemical Demineralization of Water with Porous Electrodes of Large Surface Area. In *Saline Water Conversion*, Advances in Chemistry, Vol. 27; American Chemical Society, 1960; pp 206-223.

(4) Oren, Y.; Soffer, A. Electrochemical Parametric Pumping. *Journal of The Electrochemical Society* **1978**, *125* (6), 869. DOI: 10.1149/1.2131570.

(5) Farmer, J. C.; Fix, D. V.; Mack, G. V.; Pekala, R. W.; Poco, J. F. Capacitive Deionization of NaCl and NaNO3 Solutions with Carbon Aerogel Electrodes. *Journal of The Electrochemical Society* **1996**, *143* (1), 159. DOI: 10.1149/1.1836402.

(6) Oren, Y. Capacitive Deionization (CDI) for Desalination and Water Treatment — Past, Present and Future (a Review). *Desalination* **2008**, *228* (1-3), 10-29. DOI: 10.1016/j.desal.2007.08.005.

(7) Porada, S.; Zhao, R.; van der Wal, A.; Presser, V.; Biesheuvel, P. M. Review on the Science and Technology of Water Desalination by Capacitive Deionization. *Progress in Materials Science* **2013**, *58* (8), 1388-1442. DOI: 10.1016/j.pmatsci.2013.03.005.

(8) Sufiani, O.; Elisadiki, J.; Machunda, R. L.; Jande, Y. A. C. Modification Strategies to Enhance Electrosorption Performance of Activated Carbon Electrodes for Capacitive Deionization Applications. *Journal of Electroanalytical Chemistry* **2019**, *848*, 113328. DOI: 10.1016/j.jelechem.2019.113328.

(9) Ntakirutimana, S.; Tan, W.; Anderson, M. A.; Wang, Y. Activated Carbon Electrode Design: Engineering Tradeoff with Respect to Capacitive Deionization Performance. *Journal of The Electrochemical Society* **2020**, *167* (14), 143501. DOI: 10.1149/1945-7111/abbfd7.

(10) Vinke, P.; van der Eijk, M.; Verbree, M.; Voskamp, A. F.; van Bekkum, H. Modification of the Surfaces of a Gas-Activated Carbon and a Chemically Activated Carbon with Nitric acid, Hypochlorite, and Ammonia. *Carbon* **1994**, *32* (4), 675-686. DOI: 10.1016/0008-6223(94)90089-2.

(11) Polovina, M.; Babić, B.; Kaluderović, B.; Dekanski, A. Surface Characterization of Oxidized Activated Carbon Cloth. *Carbon* **1997**, *35* (8), 1047-1052. DOI: 10.1016/S0008-6223(97)00057-2.

(12) Moreno-Castilla, C.; Ferro-Garcia, M. A.; Joly, J. P.; Bautista-Toledo, I.; Carrasco-Marin, F.; Rivera-Utrilla, J. Activated Carbon Surface Modifications by Nitric Acid, Hydrogen Peroxide, and Ammonium Peroxydisulfate Treatments. *Langmuir* **1995**, *11* (11), 4386-4392. DOI: 10.1021/la00011a035.

(13) Hsieh, C.-T.; Teng, H. Influence of Oxygen Treatment on Electric Double-Layer Capacitance of Activated Carbon Fabrics. *Carbon* **2002**, *40* (5), 667-674. DOI: 10.1016/S0008-6223(01)00182-8.

(14) Bhatnagar, A.; Hogland, W.; Marques, M.; Sillanpää, M. An Overview of the Modification Methods of Activated Carbon for its Water Treatment Applications. *Chemical Engineering Journal* **2013**, *219*, 499-511. DOI: 10.1016/j.cej.2012.12.038.

(15) Nian, Y.-R.; Teng, H. Nitric Acid Modification of Activated Carbon Electrodes for Improvement of Electrochemical Capacitance. *Journal of The Electrochemical Society* **2002**, *149* (8), A1008. DOI: 10.1149/1.1490535.
(16) Nian, Y.-R.; Teng, H. Influence of Surface Oxides on the Impedance Behavior of Carbon-Based Electrochemical Capacitors. *Journal of Electroanalytical Chemistry* **2003**, *540*, 119-127. DOI: 10.1016/S0022-0728(02)01299-8.
(17) Qiu, C.; Jiang, L.; Gao, Y.; Sheng, L. Effects of Oxygen-Containing Functional Groups On Carbon Materials in Supercapacitors: A Review. *Materials & Design* **2023**, *230*, 111952. DOI: 10.1016/j.matdes.2023.111952.
(18) Sevilla, M.; Mokaya, R. Energy Storage Applications of Activated Carbons: Supercapacitors and Hydrogen Storage. *Energy & Environmental Science* **2014**, *7* (4), 1250-1280, 10.1039/C3EE43525C. DOI: 10.1039/C3EE43525C.
(19) Ahn, H.-J.; Lee, J.-H.; Jeong, Y.; Lee, J.-H.; Chi, C.-S.; Oh, H.-J. Nanostructured Carbon Cloth Electrode for Desalination from Aqueous Solutions. *Materials Science and Engineering: A* **2007**, *449-451*, 841-845. DOI: 10.1016/j.msea.2006.02.448.
(20) Huang, W.; Zhang, Y.; Bao, S.; Cruz, R.; Song, S. Desalination by Capacitive Deionization Process Using Nitric Acid-Modified Activated Carbon as the Electrodes. *Desalination* **2014**, *340*, 67-72. DOI: 10.1016/j.desal.2014.02.012.
(21) Wu, T.; Wang, G.; Dong, Q.; Qian, B.; Meng, Y.; Qiu, J. Asymmetric Capacitive Deionization Utilizing Nitric Acid Treated Activated Carbon Fiber as the Cathode. *Electrochimica Acta* **2015**, *176*, 426-433. DOI: 10.1016/j.electacta.2015.07.037.
(22) Gao, X.; Porada, S.; Omosebi, A.; Liu, K. L.; Biesheuvel, P. M.; Landon, J. Complementary Surface Charge for Enhanced Capacitive Deionization. *Water Research* **2016**, *92*, 275-282. DOI: 10.1016/j.watres.2016.01.048.
(23) Palakkal, V. M.; Rubio, J. E.; Lin, Y. J.; Arges, C. G. Low-Resistant Ion-Exchange Membranes for Energy Efficient Membrane Capacitive Deionization. *ACS Sustainable Chemistry & Engineering* **2018**, *6* (11), 13778-13786. DOI: 10.1021/acssuschemeng.8b01797.
(24) Laxman, K.; Kimoto, D.; Sahakyan, A.; Dutta, J. Nanoparticulate Dielectric Overlayer for Enhanced Electric Fields in a Capacitive Deionization Device. *ACS Applied Materials & Interfaces* **2018**, *10* (6), 5941-5948. DOI: 10.1021/acsami.7b16540.
(25) Toledo-Carrillo, E.; Zhang, X.; Laxman, K.; Dutta, J. Asymmetric Electrode Capacitive Deionization for Energy Efficient Desalination. *Electrochimica Acta* **2020**, *358*, 136939. DOI: 10.1016/j.electacta.2020.136939.
(26) Zhang, X.; Toledo-Carrillo, E. A.; Yu, D.; Dutta, J. Effect of Surface Charge on the Fabrication of Hierarchical Mn-Based Prussian Blue Analogue for Capacitive Desalination. *ACS Applied Materials & Interfaces* **2022**, *14* (35), 40371-40381. DOI: 10.1021/acsami.2c08192.
(27) Suss, M. E.; Porada, S.; Sun, X.; Biesheuvel, P. M.; Yoon, J.; Presser, V. Water Desalination via Capacitive Deionization: What is It and What Can We Expect from It? *Energy & Environmental Science* **2015**, *8* (8), 2296-2319. DOI: 10.1039/C5EE00519A.
(28) Kim, T.; Dykstra, J. E.; Porada, S.; van der Wal, A.; Yoon, J.; Biesheuvel, P. M. Enhanced Charge Efficiency and Reduced Energy Use in Capacitive Deionization by Increasing the Discharge Voltage. *Journal of Colloid and Interface Science* **2015**, *446*, 317-326. DOI: 10.1016/j.jcis.2014.08.041.

(29) Zhao, Y.; Hu, X.-m.; Jiang, B.-h.; Li, L. Optimization of the Operational Parameters for Desalination with Response Surface Methodology During a Capacitive Deionization Process. *Desalination* **2014**, *336*, 64-71. DOI: https://doi.org/10.1016/j.desal.2013.12.024.
(30) Li, D.; Wang, S.; Wang, G.; Li, C.; Che, X.; Wang, S.; Zhang, Y.; Qiu, J. Facile Fabrication of NiCoAl-Layered Metal Oxide/Graphene Nanosheets for Efficient Capacitive Deionization Defluorination. *ACS Applied Materials & Interfaces* **2019**, *11* (34), 31200-31209. DOI: 10.1021/acsami.9b10307.
(31) Thommes, M.; Kaneko, K.; Neimark, A. V.; Olivier, J. P.; Rodriguez-Reinoso, F.; Rouquerol, J.; Sing, K. S. W. Physisorption of Gases, With Special Reference to the Evaluation of Surface Area and Pore Size Distribution. **2015**, *87* (9-10), 1051-1069. DOI: 10.1515/pac-2014-1117 (acccessed 2024-08-08).
(32) Boehm, H. P. Some Aspects of the Surface Chemistry of Carbon Blacks and Other Carbons. *Carbon* **1994**, *32* (5), 759-769. DOI: 10.1016/0008-6223(94)90031-0.
(33) Wang, X.; Cheng, H.; Ye, G.; Fan, J.; Yao, F.; Wang, Y.; Jiao, Y.; Zhu, W.; Huang, H.; Ye, D. Key Factors and Primary Modification Methods of Activated Carbon and Their Application in Adsorption of Carbon-Based Gases: A Review. *Chemosphere* **2022**, *287*, 131995. DOI: 10.1016/j.chemosphere.2021.131995.
(34) Bard, A. J.; Faulkner, L. R.; White, H. S. *Electrochemical Methods: Fundamentals and Applications*, Third edition ed.; Wiley, 2022.
(35) Chen, J. P.; Wu. Acid/Base-Treated Activated Carbons: Characterization of Functional Groups and Metal Adsorptive Properties. *Langmuir* **2004**, *20* (6), 2233-2242. DOI: 10.1021/la0348463.
(36) Chingombe, P.; Saha, B.; Wakeman, R. J. Surface Modification and Characterisation of a Coal-Based Activated Carbon. *Carbon* **2005**, *43* (15), 3132-3143. DOI: 10.1016/j.carbon.2005.06.021.
(37) Ternero-Hidalgo, J. J.; Rosas, J. M.; Palomo, J.; Valero-Romero, M. J.; Rodríguez-Mirasol, J.; Cordero, T. Functionalization of Activated Carbons by HNO3 Treatment: Influence of Phosphorus Surface Groups. *Carbon* **2016**, *101*, 409-419. DOI: 10.1016/j.carbon.2016.02.015.
(38) Kim, J.-H.; Hwang, S. Y.; Park, J. E.; Lee, G. B.; Kim, H.; Kim, S.; Hong, B. U. Impact of the Oxygen Functional Group of Nitric Acid-Treated Activated Carbon on KOH Activation Reaction. *Carbon Letters* **2019**, *29* (3), 281-287. DOI: 10.1007/s42823-019-00024-0.
(39) Pels, J. R.; Kapteijn, F.; Moulijn, J. A.; Zhu, Q.; Thomas, K. M. Evolution of Nitrogen Functionalities in Carbonaceous Materials During Pyrolysis. *Carbon* **1995**, *33* (11), 1641-1653. DOI: 10.1016/0008-6223(95)00154-6.
(40) Cordero-Lanzac, T.; Rosas, J. M.; García-Mateos, F. J.; Ternero-Hidalgo, J. J.; Palomo, J.; Rodríguez-Mirasol, J.; Cordero, T. Role of Different Nitrogen Functionalities on the Electrochemical Performance of Activated Carbons. *Carbon* **2018**, *126*, 65-76. DOI: 10.1016/j.carbon.2017.09.092.
(41) Jansen, R. J. J.; van Bekkum, H. XPS of Nitrogen-Containing Functional Groups on Activated Carbon. *Carbon* **1995**, *33* (8), 1021-1027. DOI: 10.1016/0008-6223(95)00030-H.
(42) Wang, Y.; Song, Y.; Xia, Y. Electrochemical Capacitors: Mechanism, Materials, Systems, Characterization and Applications. *Chemical Society Reviews* **2016**, *45* (21), 5925-5950, 10.1039/C5CS00580A. DOI: 10.1039/C5CS00580A.

(43) Yan, J.; Wang, Q.; Wei, T.; Fan, Z. Recent Advances in Design and Fabrication of Electrochemical Supercapacitors with High Energy Densities. *Advanced Energy Materials* **2014**, *4* (4), 1300816. DOI: 10.1002/aenm.201300816.
(44) Hulicova-Jurcakova, D.; Seredych, M.; Lu, G. Q.; Bandosz, T. J. Combined Effect of Nitrogen- and Oxygen-Containing Functional Groups of Microporous Activated Carbon on its Electrochemical Performance in Supercapacitors. *Advanced Functional Materials* **2009**, *19* (3), 438-447. DOI: 10.1002/adfm.200801236.
(45) Kim, T.; Yoon, J. Relationship Between Capacitance of Activated Carbon Composite Electrodes Measured at a Low Electrolyte Concentration and their Desalination Performance in Capacitive Deionization. *Journal of Electroanalytical Chemistry* **2013**, *704*, 169-174. DOI: 10.1016/j.jelechem.2013.07.003.
(46) Béguin, F.; Presser, V.; Balducci, A.; Frackowiak, E. Carbons and Electrolytes for Advanced Supercapacitors. *Advanced Materials* **2014**, *26* (14), 2219-2251. DOI: https://doi.org/10.1002/adma.201304137.
(47) Shi, H. Activated Carbons and Double Layer Capacitance. *Electrochimica Acta* **1996**, *41* (10), 1633-1639. DOI: 10.1016/0013-4686(95)00416-5.
(48) Barbieri, O.; Hahn, M.; Herzog, A.; Kötz, R. Capacitance Limits of High Surface Area Activated Carbons for Double Layer Capacitors. *Carbon* **2005**, *43* (6), 1303-1310. DOI: 10.1016/j.carbon.2005.01.001.
(49) Lin, F.; Xu, M.; Ramasamy, K. K.; Li, Z.; Klinger, J. L.; Schaidle, J. A.; Wang, H. Catalyst Deactivation and Its Mitigation during Catalytic Conversions of Biomass. *ACS Catalysis* **2022**, *12* (21), 13555-13599. DOI: 10.1021/acscatal.2c02074.
(50) Pandolfo, A. G.; Hollenkamp, A. F. Carbon Properties and Their Role in Supercapacitors. *Journal of Power Sources* **2006**, *157* (1), 11-27. DOI: 10.1016/j.jpowsour.2006.02.065.
(51) Valentino, L.; Alejandre, A. Capacitive Deionization for the Extraction and Recovery of Butyrate. *ACS Sustainable Chemistry & Engineering* **2023**, *11* (16), 6385-6394. DOI: 10.1021/acssuschemeng.3c00221.

TOC/ABSTRACT GRAHPIC

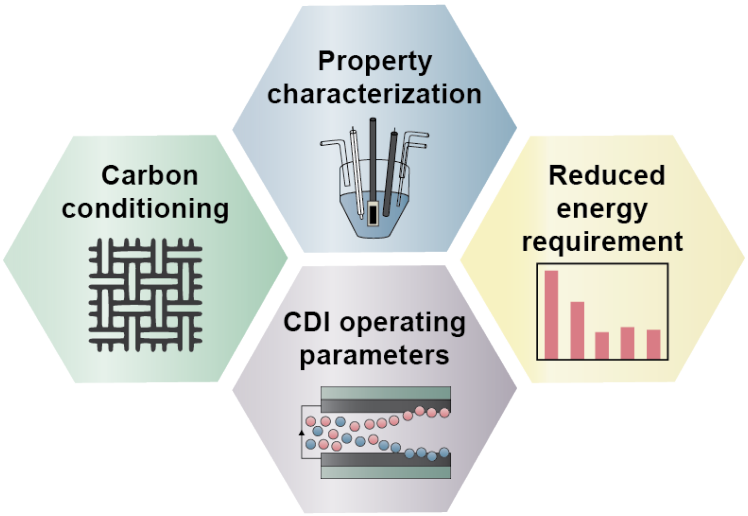

SYNOPSIS

This study reduces CDI energy consumption by 3.8× through a combination of electrode pretreatment and tuning of operating parameters.